Earth and Planetary Science Letters 363 (2013) 109–120

Contents lists available at SciVerse ScienceDirect

Earth and Planetary Science Letters

journal homepage: www.elsevier.com/locate/epsl

Crustal manifestations of a hot transient pulse at 60°N beneath the Mid-Atlantic Ridge

R.E. Parnell-Turner [a,*], N.J. White [a], J. Maclennan [a], T.J. Henstock [b], B.J. Murton [c], S.M. Jones [d]

[a] Bullard Laboratories, Department of Earth Sciences, University of Cambridge, Cambridge CB3 0EZ, UK
[b] National Oceanography Centre Southampton, University of Southampton, European Way, Southampton SO14 3ZH, UK
[c] National Oceanography Centre, European Way, Southampton SO14 3ZH, UK
[d] School of Geography, Earth and Environmental Sciences, University of Birmingham, Edgbaston B15 2TT, UK

ARTICLE INFO

Article history:
Received 30 August 2012
Received in revised form
21 December 2012
Accepted 26 December 2012
Editor: P. Shearer

Keywords:
mantle convection
Atlantic Ridge
Iceland
plume
normal faulting
volcanism

ABSTRACT

Since its inception at 62 Ma, mantle convective upwelling beneath Iceland has had a significant influence on Cenozoic vertical motions, magmatism and paleoceanography in the North Atlantic Ocean. Crucially, intersection of the Reykjanes Ridge with the Icelandic Plume provides us with a useful window into the transient activity of this plume. Here, the spreading ridge acts as a linear sampler of plume activity, which is recorded as a series of time-transgressive V-shaped ridges and troughs. We present the results of a detailed study of the spreading ridge close to 60°N, where the youngest V-shaped ridge of thickened oceanic crust is forming today. A combination of multibeam bathymetry and seismic reflection profiles, acquired along and across the ridge axis, is used to map the detailed pattern of volcanism and normal faulting. Along the ridge axis, the density of volcanic seamounts varies markedly, increasing by a factor of two between 59°N and 62°N. Within this zone, seismic imaging shows that there is enhanced acoustic scattering at the seabed. These observations are accompanied by a decrease in mean fault length from ~12 km to ~6 km. A 1960–2009 catalog of relocated teleseismic earthquake hypocenters indicates that there is a pronounced gap in seismicity between 59°N and 62°N where the cumulative moment release is two orders of magnitude smaller than that along adjacent ridge segments. A steady-state thermal model is used to show that a combination of increased melt generation and decreased hydrothermal circulation accounts for this suite of observations. The predicted decrease in the thickness of the brittle seismogenic layer is consistent with geochemical modeling of dredged basaltic samples, which require hotter asthenospheric material beneath the spreading axis. Thus, along-axis variation in melt supply caused by passage of a pulse of hot material modulates crustal accretion processes and rheological properties.

© 2013 Elsevier B.V. All rights reserved.

1. Introduction

It is widely accepted that convective circulation of the Earth's mantle modifies surface elevation (e.g. Schubert et al., 2001). Elevation change produced in this way is referred to as dynamic topography in order to distinguish it from isostatic topography which is maintained by changes in the density structure of the lithosphere (Hager et al., 1985; Hager and Richards, 1989; Cazenave et al., 1989). Spatial and temporal variations in dynamic topography play an important role in sculpting terrestrial landscapes and in moderating deep-water overflow at oceanic gateways (Wright and Miller, 1996; Jones et al., 2001; Poore et al., 2006). The North Atlantic Ocean is an important natural laboratory where the behavior of time-dependent convective circulation can be investigated in diverse ways. Here, hot plume material is thought to rise within a conduit located beneath Iceland and spread outward beneath the lithospheric plate (White, 1997; Delorey et al., 2007). Marine geophysical observations combined with a fluid dynamical understanding of convective upwelling suggest that periodic oscillations within the plume's conduit trigger transient temperature fluctuations which spread out horizontally over large distances (Schubert and Olson, 1989; White et al., 1995; Ito, 2001; Jones et al., 2002b). These fluctuations are manifest in different ways: variations in the thickness and composition of oceanic crust; changes in the overflow of North Atlantic Deep Water across the Greenland–Scotland Ridge; and periodic development of ancient ephemeral landscapes (Jones et al., 2002b; Poore et al., 2011; Hartley et al., 2011).

South of Iceland, the Reykjanes Ridge is an oblique and slow spreading axis, which is uninterrupted by fracture zones (Fig. 1). This ridge is flanked by a series of diachronous V-shaped ridges, which was first described by Vogt (1971). At 60.3°N, the youngest

* Corresponding author. Tel.: +44 1223 337064; fax: +44 1223 360779.
E-mail address: rep52@cam.ac.uk (R.E. Parnell-Turner).

0012-821X/$ - see front matter © 2013 Elsevier B.V. All rights reserved.
http://dx.doi.org/10.1016/j.epsl.2012.12.030

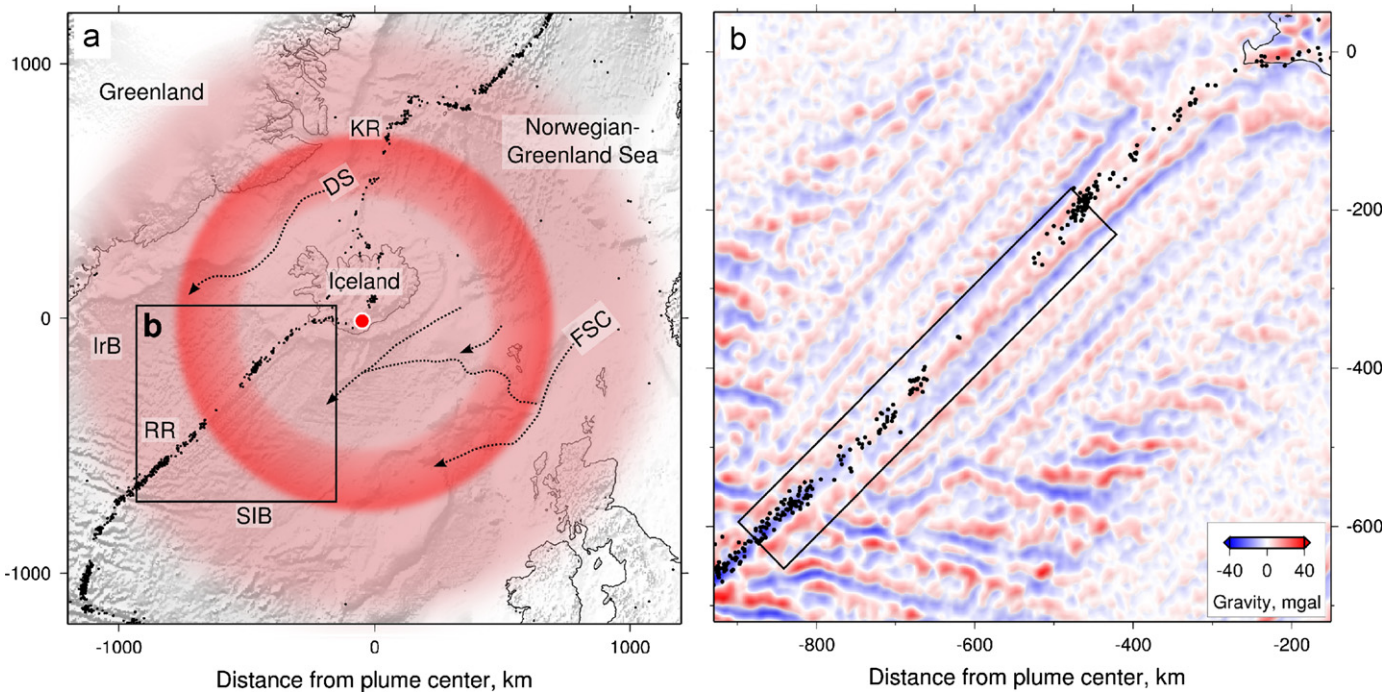

Fig. 1. (a) Bathymetric map of North Atlantic Ocean showing idealized extent of Icelandic Plume (projection centered on 63.95°N, 17.4°W). Transparent red disk, present-day extent of plume; red ring, radial locus of transient thermal anomaly inferred at intersection of youngest V-shaped ridge with RR; small red circle, plume center (Shorttle et al., 2010); black circles, relocated earthquakes for 1960–2009 (magnitude >4; Engdahl et al., 1998). IrB, Irminger Basin; RR, Reykjanes Ridge; SIB, South Iceland Basin; KR, Kolbeinsey Ridge; labeled dashed lines, deep-water pathways (FSC, Faroe–Shetland Channel overflow; DS, Denmark Straits overflow); black box, location of Fig. 1b. (b) Short wavelength free-air gravity map of North Atlantic Ocean calculated from satellite-derived data by removing wavelengths greater than 100 km (Sandwell and Smith, 2009). Box, location of Figs. 2a and 3. (For interpretation of the references to color in this figure legend, the reader is referred to the web version of this article.)

V-shaped ridge meets the ridge axis where the crustal thickness measured in a wide-angle seismic experiment is 10.0 ± 0.5 km (Smallwood and White, 1998). At 58.5°N, the adjacent trough has a projected crustal thickness of 7.8 ± 0.5 km. Along the ridge axis itself, systematic variations in major, trace and rare earth elemental compositions from dredged basaltic rocks correspond to the intersections of V-shaped ridges and troughs (Murton et al., 2002; Jones et al., 2010; Poore et al., 2011). These crustal thickness and geochemical variations are best explained by 25–30 °C fluctuations in the asthenospheric potential temperature (White et al., 1995; Poore et al., 2011). A suite of different geophysical, geochemical and paleoceanographic observations support the existence of transient thermal anomalies which are generated within the plume conduit and flow outward within a horizontal channel (e.g. Vogt, 1971; White, 1997; Ito, 2001; Jones et al., 2002b). Closer to Iceland, high resolution magnetic and bathymetric profiles imply that asymmetric spreading occurs over the last 15 Ma (Hey et al., 2010; Benediktsdóttir et al., 2012). This asymmetry could be accounted for by progressive eastward stepping of the propagating Reykjanes Ridge. In the last 6 Ma, there is little evidence for asymmetry within the uncertainty of the magnetic anomaly picks (Benediktsdóttir et al., 2012). Crustal thickness and geochemical variations along the spreading axis itself cannot be easily accounted for by the effects of ridge propagation.

A V-shaped ridge is currently forming at the spreading axis and its tip occurs at 60°N, ~760 km southwest of Iceland (Fig. 1). The detailed structure of this nascent V-shaped ridge implies that a hot, transient anomaly is propagating away from Iceland at the present day (Searle et al., 1998). A combination of multibeam bathymetric and seismic reflection profiles acquired on this segment of the Reykjanes Ridge enables us to investigate how this anomaly has influenced the structure and evolution of the brittle crust. By combining this analysis with the distribution of teleseismically recorded earthquakes and with the geochemistry of dredged basaltic rocks, we develop a better understanding of how horizontally advecting thermal anomalies modify oceanic crust. A steady-state thermal model of the spreading axis is used to explore the relationship between brittle deformation, hydrothermal circulation, rheological structure, and crustal accretion processes at this slow-spreading ridge (e.g. Chen, 2003; Buck et al., 2005; Behn and Ito, 2008; Ito and Behn, 2008).

2. Multibeam bathymetry

Bathymetric surveys were acquired during Cruise JC50 on the RRS *James Cook* during July–August 2010. At the Reykjanes Ridge, bathymetric profiles were collected along four flowlines which straddle the ridge centered at 60°N and 61.5°N (Fig. 2). Additional profiles were collected along the ridge crest itself. These data were acquired using a hull-mounted Kongsberg EM120 multibeam echo sounder operating at a frequency of 12 kHz with a swath width which is ~6 times the average water depth.

Processing was carried out using the Caris HIPS software and a gridded dataset that covers $>28{,}000$ km^2 was generated. Here, we exploit a subset that consists of 1293 km^2 acquired at the ridge crest. The horizontal resolution is ~30 m. This survey overlaps with regionally extensive surveys acquired on Cruise EW9008 (RV *Maurice Ewing*; Searle et al., 1994) and on Cruises CD81 and CD87 (RRS *Charles Darwin*; Keeton et al., 1997). The average horizontal resolution of these earlier surveys is ~100 m.

2.1. Volcanism

Morphology of the Reykjanes Ridge is dominated by an axial high which is characterized by a series of *en echelon* axial volcanic

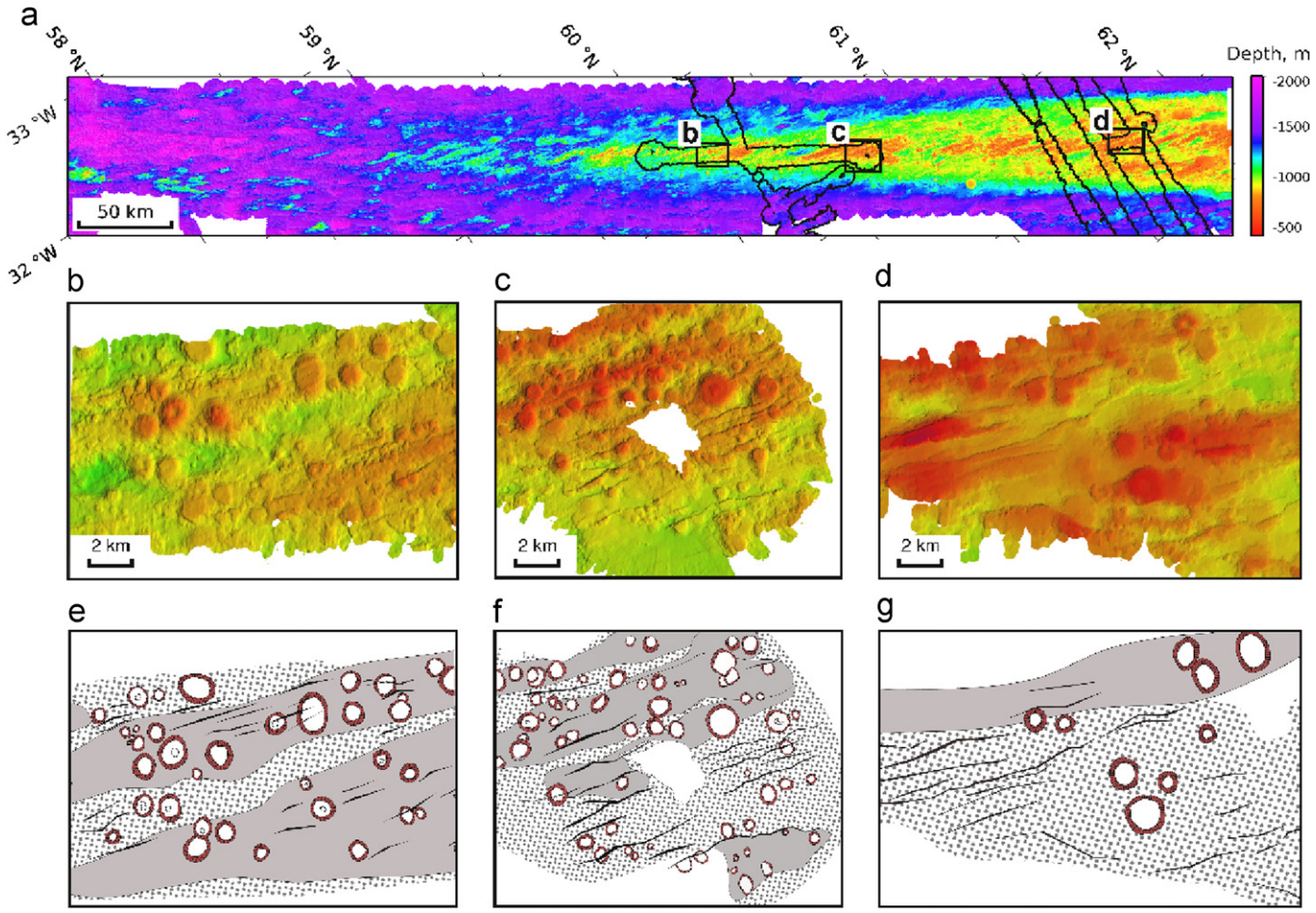

Fig. 2. Bathymetry of Reykjanes Ridge. (a) Bathymetric map showing combined multibeam bathymetric data (Cruises CD87 and JC50; Fig. 1). Irregular polygons, location of high resolution bathymetry acquired during Cruise JC50. (b)–(d) Detailed bathymetric images from Cruise JC50. (e)–(g) Geologic interpretations. Circles with brown hachured slopes, seamounts; black lines, normal faults; gray polygons, AVRs; stippled areas, hummocky volcanic terrains. (For interpretation of the references to color in this figure legend, the reader is referred to the web version of this article.)

ridges (AVRs). These AVRs are covered with circular volcanic seamounts, which often overlap each other and are occasionally dissected by normal faults (Fig. 2). These seamounts have diameters of ~2 km and heights of 200–300 m. Sometimes they are dimpled with craters, which have depths of more than 100 m. Seamounts are mostly concentrated at the ridge axis and are less apparent at distances greater than ~10 km from the axis, probably as a result of sedimentary blanketing and normal faulting. The biggest AVR in the study area has a relief of ~400 m and a width of 6.5 km (Fig. 2c). Its rugged surface is covered with many hummocky and flat-topped seamounts. Detailed interpretations of selected portions of the ridge axis are shown in Fig. 2e–g. Using the criteria of Smith and Cann (1992), 205 seamounts were identified within the study region. Of these, 120 (59%) are smooth and 84 (41%) are hummocky, which is consistent with the study of Magde and Smith (1995), who used side-scan sonar images from a 140 km segment of the ridge axis at 60°N. However, there is a marked difference in the abundance of seamounts and in seabed morphology along the ridge axis. There is a higher density of seamounts further south (Fig. 2b–c). Many seamounts have craters and the seabed is characterized by short wavelength hummocky features. Further north, the density of seamounts is considerably reduced and the seabed is smoother (Fig. 2d). These results are consistent with the bathymetric study of Appelgate and Shor (1994), who analyzed seamount density between 56°N and 63°N (Fig. 7c). They showed that the maximum seamount density occurs at 60°N.

2.2. Tectonic structure

Normal faulting occurs along the length of the ridge axis but its style and distribution changes markedly as a function of distance (Searle et al., 1998; Figs. 2 and 3b). To ensure self-consistency, we have reinterpreted fault scarps between ~57°N and 63°N using the lower resolution bathymetric survey from Cruise CD87 (Fig. 3b; Keeton et al., 1997). The largest number of faults occurs south of 59.5°N, where fault scarps have displacements of >200 m and fault lengths range from 2 to 30 km with a mean value of 12 km. Fault density (i.e. cumulative fault length) is 120 m km^{-2}. North of 59.5°N and south of 61.5°N, mean fault length halves to ~6 km, fault density drops to 40 m km^{-2}, and fault displacement is less than 200 m. North of 61.5°N, mean fault length increases to 7 km and fault density doubles to 80 m km^{-2}.

These results are borne out by higher resolution bathymetric images (Fig. 2). North of 61.5°N, long sinuous normal faults with strike lengths of up to 12 km are visible (Fig. 2d). Further south, the average strike length is smaller (~6 km). In both cases, fault displacements are ~100 m. This dramatic change in both the distribution and style of faulting between 59.5°N and 61.5°N coincides with the intersection between the youngest V-shaped ridge and the spreading axis. The coincidence suggests that thermomechanical properties of the upper crust have been altered by the presence of a thermal anomaly beneath the spreading axis.

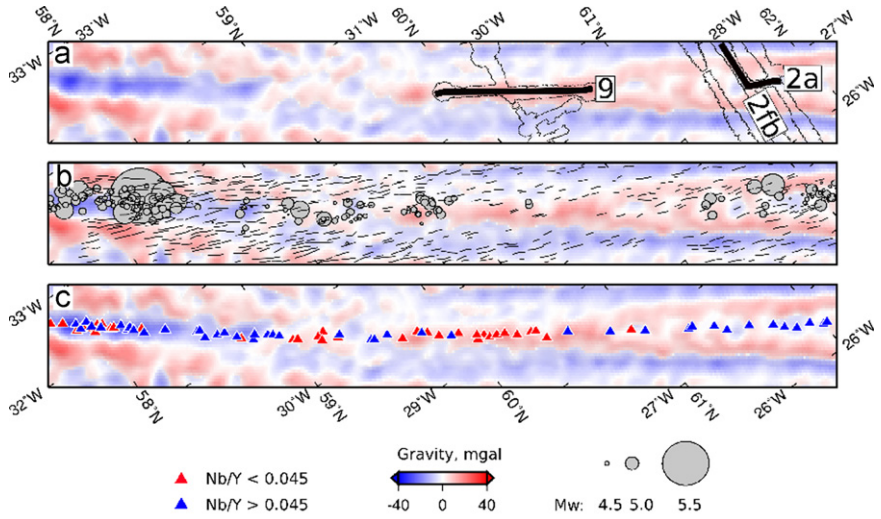

Fig. 3. Geologic observations along, and adjacent to, Reykjanes Ridge overlain on short wavelength gravity anomalies (Fig. 1). (a) Location of selected bathymetric and seismic profiles acquired during Cruise JC50. Irregular polygons, high resolution bathymetry; labeled black lines, two-dimensional seismic reflection profiles shown in Figs. 5 and 6. (b) Distribution of earthquakes and normal faults. Gray circles, scaled magnitudes of earthquakes from 1960 to 2009 (Engdahl et al., 1998); black lines, normal faults mapped on bathymetric data (Keeton et al., 1997). (c) Geochemistry of dredged basalts (Murton et al., 2002). Blue triangles, Nb/Y >0.045; red triangles, Nb/Y <0.045. (For interpretation of the references to color in this figure legend, the reader is referred to the web version of this article.)

3. Seismic reflection imaging

A set of regional seismic reflection profiles was also acquired as part of Cruise JC50. The centerpiece of this survey is a pair of flowlines, which traverse the oceanic basin from the European Shelf to the Greenland Shelf and will enable us to elucidate the history of V-shaped ridge activity for the last 50 Ma (Parnell-Turner et al., 2011). A small fraction of this survey was acquired along and adjacent to the mid-oceanic ridge between 60°N and 62°N (Fig. 3a). These data were acquired using a single generator–injector airgun (generator pulse=4.1 l, injector pulse=1.7 l) fired every 15 s at a pressure of 20.7 MPa. A 1600 m streamer with a group interval of 12.5 m and a near offset of 163 m was deployed. Nominal ship speed was 5 knots (i.e. 2.6 m/s), which yields a shot spacing of $\sim$40 m and a fold of cover of $\sim$21. A standard signal processing sequence was used. After sorting into common mid-point gathers, a low-cut Butterworth filter with a cut-off frequency of 12 Hz and a slope of 24 dB/octave was applied to remove incoherent noise. Stacking velocities were picked every 625 m using a combination of semblance analyses and constant velocity stacking panels. A post-stack Stolt migration was carried out with a constant velocity of 1500 m s^{-1}.

By combining bathymetric and seismic datasets, the three-dimensional geometry of AVRs and their constituent volcanic edifices can be clearly imaged (Figs. 5 and 6). Three prominent AVRs are visible at the southern end of the survey. Seamounts with craters are also visible (Fig. 5b). Rugose bathymetry along the ridge axis scatters acoustic energy from the seabed and generates steeply dipping, out-of-the-plane reflections which pervade the seismic image (Calvert, 1997; Peirce et al., 2007). Scattered energy is particularly evident at 60°N where a greater density of volcanic edifices has produced highly variable bathymetry.

The seismic experiment has a small aperture and was designed to image the sediment–basement interface. Consequently, the ability to image upper crustal reflectivity is compromised. Nonetheless, there is some evidence for coherent reflectivity beneath the seabed. A discontinuous reflection is seen on profiles which traverse the ridge crest. It may correspond to the base of layer 2A, which delineates either the boundary between pillow basalts and intrusive dykes or the depth of penetration of hydrothermal circulation (Harding et al., 1993; Canales et al., 2005; Vera et al., 1990; Christeson et al., 2007). At the southern end of the survey, this putative layer 2A is thicker since a reflection occurs $\sim$0.2 s below the seabed (Fig. 5). Its discontinuous character is probably due to seabed scattering. Further north, this layer is thinner and is marked by a more continuous reflection with a larger amplitude $\sim$0.1 s beneath the seabed (Fig. 6).

Along the ridge axis between 61.5°N and 62°N, Smallwood and White (1998) estimated the thickness of layer 2A from the arrival times of two distinctive refracted phases. They obtained a mean thickness of 400 ± 130 m with an indication that layer 2A is thicker beneath AVRs. Changes in the thickness and character of layer 2A at zero age have also been documented further south. For example, Peirce et al. (2007) report thicknesses of 130–200 m on depth-converted seismic reflection profiles at 57.75°N. If the base of layer 2A corresponds to the transition from lavas to sheeted dykes, an apparent thickening at 60°N could be caused by increased production of extrusive pillow basalts. It is less likely that sporadically observed reflections represent an alteration front controlled by the depth of hydrothermal circulation since normal faulting is less abundant.

4. Earthquake seismicity

The spatial and temporal distribution of earthquake seismicity at, and away from, mid-oceanic ridges yields useful information about the thermomechanical properties of oceanic lithosphere (Wiens and Stein, 1983). Here, along-axis changes in seismicity are used to investigate the brittle-plastic transition beneath the spreading center (Toomey et al., 1985; Huang and Solomon, 1988). We exploit a database of relocated teleseismic earthquake hypocenters from 1960 to 2009 (Engdahl et al., 1998). Fig. 1 shows location of earthquake hypocenters with magnitudes of greater than 4.0, which occur within 35 km of the ridge crest. Two noticeable gaps in seismicity, which are significantly wider than epicentral uncertainty, occur either side of Iceland. Each gap starts and ends at radial distances of 530 and 760 km from the plume center (Shorttle et al., 2010).

The seismicity along the Reykjanes Ridge is shown in Fig. 3b. South of 60°N, a region of intense seismicity occurs, which has

numerous on-axis events with body wave magnitudes, m_b, of up to 5.6. Seismicity peters out north of a prominent fracture zone at a morphological change from median valley to axial high at 58.8°N. North of 60°N, there is a dramatic reduction in seismicity where only two earthquakes have been reported along the ridge south of 61.5°N. This gap was tentatively identified by Francis (1973) and Einarsson (1979) using a smaller database of poorly located earthquakes. North of 61.5°N, sparse seismicity returns.

We have estimated seismic moment, M_0, between 1960 and 2009 from the moment magnitude of each earthquake using the scalar relationships of Hanks and Kanamori (1979), Kanamori (1983) and Hanks and Boore (1984). As expected, cumulative seismic moment varies markedly along the ridge (Fig. 7b). The largest drop occurs at 58.5°N where M_0 decreases by a factor of greater than two. Between 60° and 61.3°N, M_0 is negligible. Although M_0 increases after 61.3°N, it remains small. This pattern is consistent with the temporal and spatial variation in seismicity along axis. Correlation between the seismic gap and the density of normal faulting suggests that the paucity of earthquakes does not reflect an undersampling of earthquake repeat times. Furthermore, the reappearance of minor seismicity north of 61.3°N suggests that earthquake activity along the ridge is not solely a function of proximity to the Icelandic Plume. On Iceland itself, it is important to note that the biggest earthquakes occur in the Vatnajökull area and along two transform faults, which transfer spreading from the active Northern and Eastern Volcanic Zones out onto mid-oceanic ridges (Einarsson, 1991). Away from these locations, seismicity is diminished (but not negligible), which suggests that the seismic gaps on either side of Iceland are related to transient anomalies within the head of the plume.

The seismic moment of individual earthquakes can be used to estimate changes in rupture radius, a, along the Reykjanes Ridge. Following Eshelby (1957), we assume that a fault can be approximated by a circular crack which yields

$$M_0 = \frac{16}{7}\Delta\sigma a^3 \quad (1)$$

where $\Delta\sigma$ is the constant stress drop along a given ridge axis. The variation of a along the Reykjanes Ridge is shown in Fig. 4b. If $\Delta\sigma = 3$ MPa, an earthquake with M_w=4.5, which is typical of the area around 60°N, has a rupture radius of $\sim$1 km (Hanks, 1977). If M_w=5.2, which is typical of the ridge further north and south, the rupture radius is $\sim$2.2 km. These rule-of-thumb estimates are consistent with variations in the average strike lengths of normal faults (Fig. 4a).

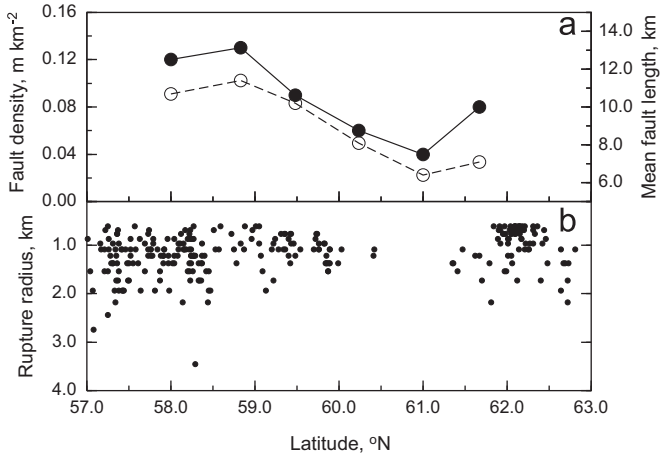

Fig. 4. Fault characteristics as a function of distance along Reykjanes Ridge. (a) Fault scarp lengths mapped on bathymetric data in 100 km bins (Cruise CD87). Solid circles, fault density, m km^{-2}; open circles, mean fault length. (b) Calculated rupture radii of earthquakes with magnitude >4 (Engdahl et al., 1998).

5. Basaltic geochemistry and crustal thickness

Basaltic rocks have been dredged along the Reykjanes Ridge between 57.3°N and 63°N (Murton et al., 2002). Major, trace, and rare earth elemental measurements show that the composition of these basaltic rocks varies along the ridge axis (Fig. 7e). The trace elemental ratio, Nb/Y, is a convenient representation of this variation because it is insensitive to crustal fractionation processes. Instead, Nb/Y reflects melt composition, which is determined either by mantle source composition or by depth and degree of melting. The southward decrease of Nb/Y between 63°N and 61°N matches deepening of the mid-oceanic ridge, with a gradual decrease in crustal thickness, and with decreasing source enrichment calculated from isotopic measurements (e.g. $^{87}Sr/^{86}Sr$). Geochemical enrichment closer to Iceland is caused by melting of compositional heterogeneities within the plume conduit (Shorttle and Maclennan, 2011). Southward flow along the ridge axis progressively melts out these heterogeneities. Fig. 7e also highlights a shorter wavelength chemical variation, which is evident in a suite of major, trace, and rare earth elements. This variation correlates with the pattern of V-shaped ridges.

At 63.3°N, where the youngest V-shaped ridge intersects the ridge axis, there is a minimum in Nb/Y and the crustal thickness measured in a seismic wide-angle experiment is 10.0 ± 0.5 km (Smallwood and White, 1998). At 58.5°N, the V-shaped trough has a projected crustal thickness of 7.8 ± 0.5 km. Thus thicker oceanic crust correlates with lower Nb/Y, with lower values of other trace elemental ratios, and with lower concentrations of incompatible elements. Thinner oceanic crust correlates with higher Nb/Y and with higher concentrations of incompatible elements. This negative correlation is inconsistent with an exclusively compositional origin for V-shaped ridges and troughs since melting of enriched portions of mantle beneath the ridge should generate thicker crust. Instead, Poore et al. (2011) showed that the chemical variation south of 61°N must be predominantly controlled by changes in asthenospheric temperature. Their one-dimensional modeling of trace and rare earth elements at 60.3°N and 59°N suggests that asthenospheric temperature changes by 25 °C.

6. Crustal magnetization

Using magnetic data acquired during Cruise CD87, Lee and Searle (2000) developed a three-dimensional inverse model with a 500 m thick magnetic source layer to show that significant along-axis variations in crustal magnetization occur (Fig. 7a). The axial zone is characterized by a central anomaly magnetic high which is commonly observed along mid-oceanic ridges. This high is attributed to the presence of recently emplaced, highly magnetic lavas. Their magnetization is attributed to titanomagnetite in young pillow basalts, which were erupted in the last 800 kyrs when geomagnetic paleointensity has been large and positive (Marshall and Cox, 1972; Klitgord, 1976). Lee and Searle (2000) also report variations in the amplitude and regularity of magnetization along the ridge axis (Fig. 7a). For example, the axial region south of 59.2°N has the largest magnetization anomaly as well as the greatest degree of irregularity, punctuated by several isolated magnetization lows. Axial magnetization is diminished between 59.2°N and 60.8°N. North of 60.8°N, axial magnetization increases, returning to values typical of central anomaly magnetic highs elsewhere.

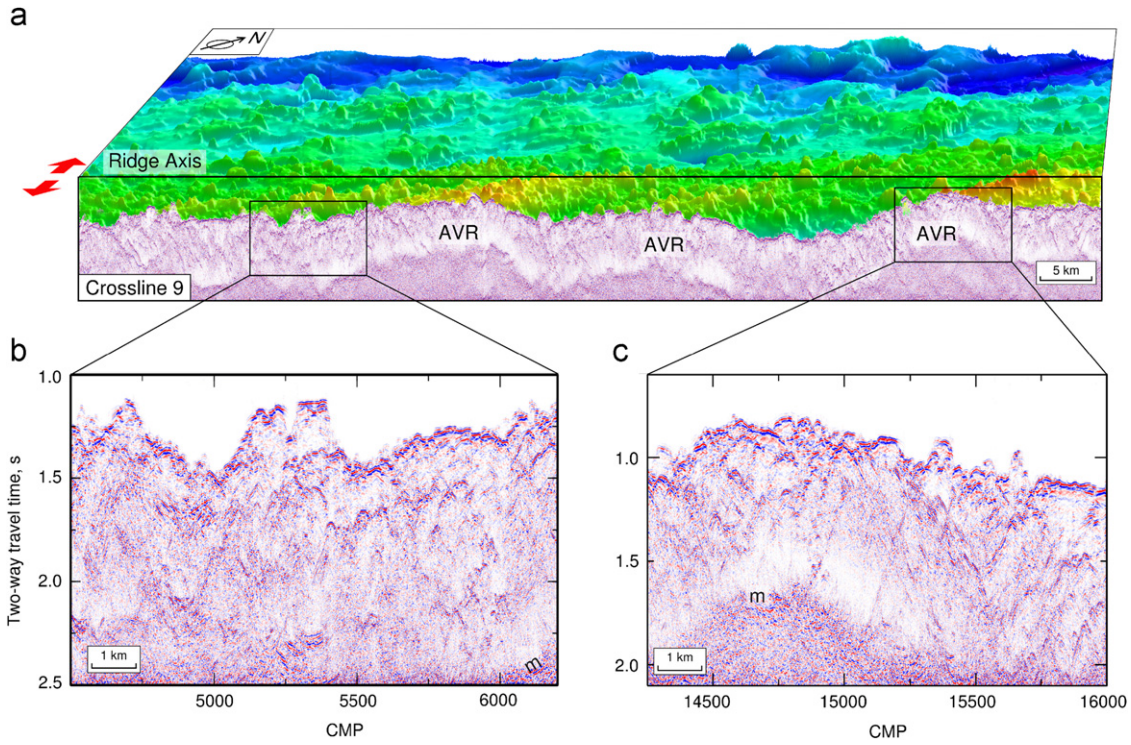

Fig. 5. (a) Three-dimensional perspective view of Reykjanes Ridge constructed from combination of bathymetric and seismic reflection data (Fig. 3). Center of view is at ~60.5°N, looking to northwest. Red arrows, plate spreading direction; AVR, loci of axial volcanic ridges. (b) and (c) Details of seismic reflection profile with examples of seamounts, sideswipe and scattered energy. sm, seamounts; m, seabed multiple. (For interpretation of the references to color in this figure legend, the reader is referred to the web version of this article.)

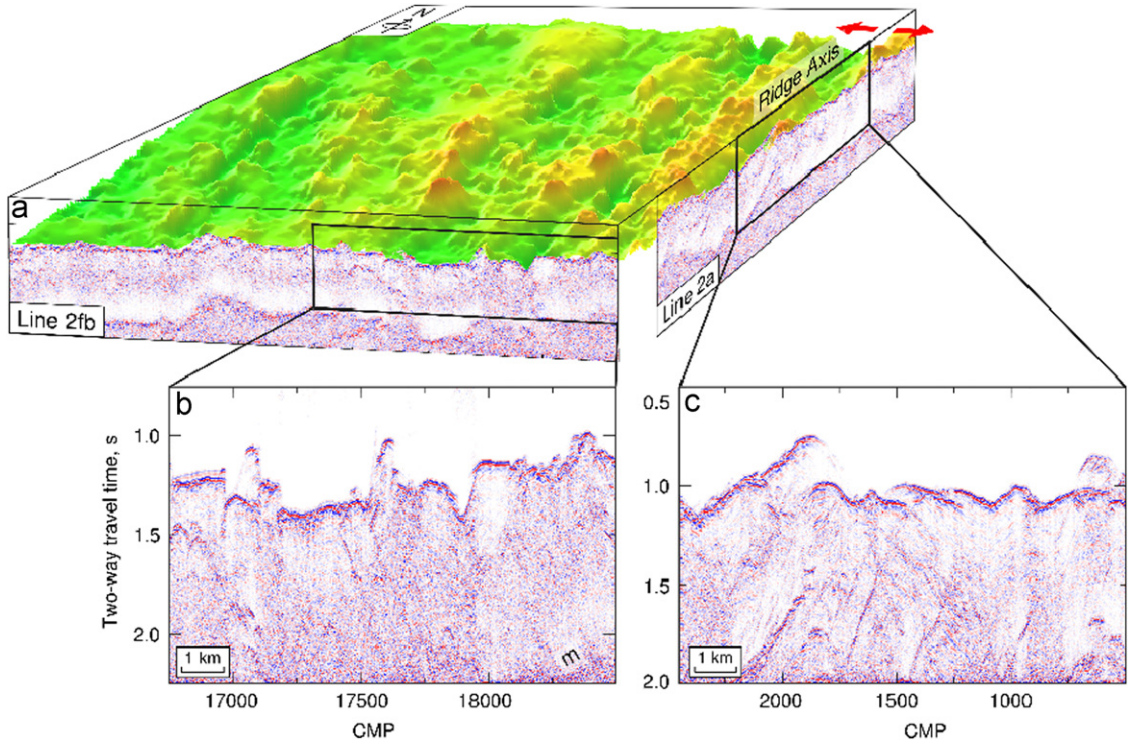

Fig. 6. (a) Three-dimensional perspective view of Reykjanes Ridge constructed from combination of multibeam bathymetric and seismic reflection data (Fig. 3). Center of view is at ~61.5°N, looking to north. Red arrows, plate spreading direction. (b) and (c) Details of seismic reflection profile. m, seabed multiple reflection. (For interpretation of the references to color in this figure legend, the reader is referred to the web version of this article.)

Lee and Searle (2000) presented a conceptual model in which the ridge axis is divided into three distinct regimes. The southern regime between 57.5°N and 59.2°N has a relatively high magnetization intensity, typical of a normal slow spreading ridge. They inferred that the central regime between 59.2°N and 60.8°N has a lower magnetization intensity because it is underlain by the

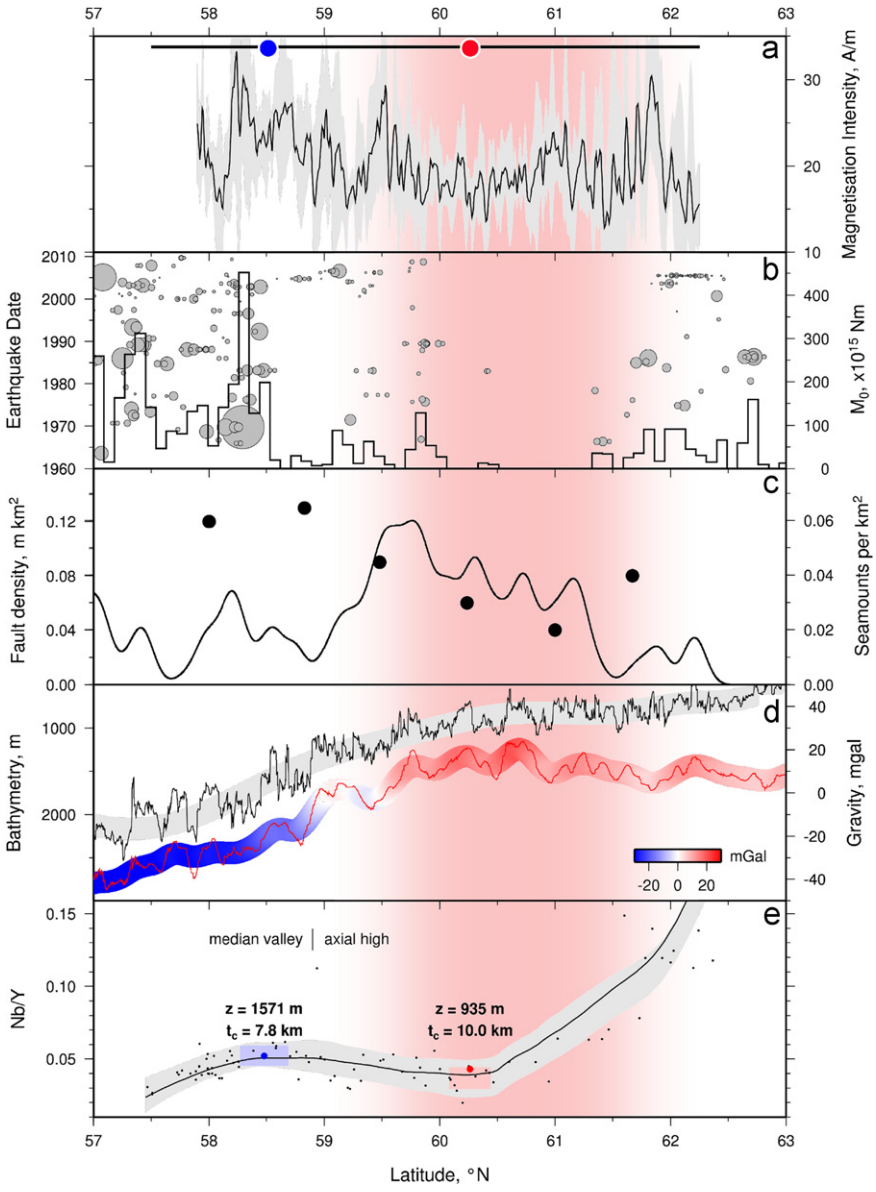

Fig. 7. Summary of geophysical/geochemical observations along Reykjanes Ridge between 57°N and 63°N. Vertical pink band delineates region where youngest VSR intersects Reykjanes Ridge. (a) Black line with gray band, intensity of magnetization $\pm 1\sigma$ along mid-oceanic ridge redrawn from Lee and Searle (2000); horizontal line along top, extent of Figs. 2 and 3. Red/blue circles, locations shown in Fig. 9. (b) Seismicity between 1960 and 2009 (Engdahl et al., 1998). Scaled gray circles, earthquakes with magnitude >4 within ± 35 km of ridge crest plotted as a function of calendar year (see Fig. 3 for magnitude scaling); black line, cumulative moment release, M_0, in 5 arc min (~ 9 km) bins. (c) Solid circles, fault density interpreted from bathymetry (Keeton et al., 1997); black line, seamount density binned every 5 arc min of latitude and smoothed with Gaussian window of 0.5° (Appelgate and Shor, 1994). (d) Black line, bathymetry, with polynomial fit; red line, high-pass, free-air gravity anomaly (Sandwell and Smith, 2009); red/blue band, 1° smoothed free-air gravity anomaly. (e) Geochemistry of dredged basalts. Black dots, measured Nb/Y (Murton et al., 2002); black line on gray band, best fitting line $\pm 1\sigma$; red/blue circles, calculated Nb/Y for $T_p = 1354$ °C and 1330 °C, respectively (Poore et al., 2011); z, bathymetry and t_c, crustal thickness at red/blue loci. (For interpretation of the references to color in this figure legend, the reader is referred to the web version of this article.)

hot plume front which has increased the rate of melt production. The northern regime has a moderate magnetization intensity. Their conceptual model is corroborated by the suite of observations summarized in Fig. 7.

Changes in the thickness of the magnetic layer could also account for variations in magnetization intensity. The model of Lee and Searle (2000) does not account for the changing frequency of seamounts and magma supply in the shallow crust. Thus minor changes in geomagnetic intensity could account for magnetization contrasts at the central magnetic anomaly high (Gee et al., 2000). Fortunately, rapid alteration processes are thought to be less important (Kent and Gee, 1996; Zhou et al., 2000). Gee et al. (2000) also showed that the paleointensity record for the past 80 kyrs can be used to explain the pattern of magnetization associated with the most recent volcanism at the ridge. Paleointensities for the past 1–3 kyrs are significantly higher than the present field value, whereas very low values are associated with the Laschamp excursion which occurred at 46.6 ± 2.4 kyr (Levi et al., 1990). Values between 80 and 46.6 kyrs are also higher. Low magnetization intensity values between 59.2°N and 60.8°N may be associated with the Laschamp excursion, which suggests that volcanism in this location occurred within the last 46.6 kyrs. Submersible dives over AVRs associated with magnetization intensity highs in the region of 59.5°N found no evidence for recent submarine volcanism, which implies that such highs are associated with older periods of volcanic activity (Crane et al., 1997).

Table 1
Constants and variables used in thermomechanical calculations.

Symbol	Description	Value	Unit	Dimension
T	Temperature	–	°C	Θ
T_l	Temperature at base of lithosphere	–	°C	Θ
t_c	Crustal thickness	–	km	L
z_l	Thickness of lithosphere	100	km	L
z_s	Depth of first melting	80	km	L
θ	Dry adiabat	0.3	K km^{-1}	Θ km^{-1}
β	Melting gradient	3.0	K km^{-1}	Θ km^{-1}
α	Liquid adiabat	1.0	K km^{-1}	Θ km^{-1}
u	Spreading half-rate	3.2×10^{-10}	m s^{-1}	L T^{-1}
ρ	Density	2.9×10^{3}	kg m^{-3}	M L^{-3}
c	Specific heat capacity	1.085×10^{3}	J kg^{-1} K^{-1}	L^2 T^{-2} Θ^{-1}
L	Latent heat	5.06×10^{5}	J kg^{-1}	L^2 T^{-2}
k	Thermal conductivity	2.5	W m^{-1} K^{-1}	M L T^{-3} Θ^{-1}
$\kappa\equiv\frac{k}{\rho c}$	Thermal diffusivity	6.7×10^{-7}	m^2 s^{-1}	L^2 T^{-1}
σ_1, σ_3	Principal stresses	–	MPa	M L^{-1} T^{-2}
R'	Ratio σ_1/σ_3	5	–	–
λ	Pore fluid factor	0.4	–	–
Q	Activation energy for creep	260	kJ mol^{-1}	M L^2 T^{-2}
R	Gas constant	8.3145	J K^{-1} mol^{-1}	M L^2 T^{-2} Θ^{-1}
A	Material strength constant	2.0×10^{-4}	MPa^{-n} s^{-1}	M L^{-1} T^{-3}
$\dot{\varepsilon}$	Strain rate	10^{-15}	s^{-1}	T^{-1}
n	Power law exponent	3.4	–	–

7. Thermal model

We describe and apply a simple thermal model which can be used to account for the changing pattern of volcanism, faulting and seismicity along the Reykjanes Ridge between 57°N and 63°N. Our main objective is to show that modest fluctuations in asthenospheric temperature at the ridge axis alter the thermal and rheological structure of oceanic crust in a significant way.

At a mid-oceanic ridge, the steady-state temperature field, $T(x,z)$, must satisfy

$$u\frac{\partial T}{\partial x}=\kappa\left(\frac{\partial^2 T}{\partial x^2}+\frac{\partial^2 T}{\partial z^2}\right)+Q(x,z) \tag{2}$$

where u is the half-spreading rate, T is the temperature, x is the distance from ridge, z is the depth, κ is the thermal diffusivity, and Q represents the heat sources and sinks which arise from latent heat and hydrothermal circulation (Table 1, Sleep, 1974, 1975; Morton and Sleep, 1985). This equation can be solved in two stages (see Appendix A for further details). First, we consider the heat source provided by magmatic intrusion at the ridge axis. Eq. (2) is solved using the approach of Sleep (1975) who explicitly included the effects of latent heat generated by adiabatic melting of vertically advecting mantle material and by later solidification of basaltic crust. Second, we determine the temperature field generated by off-axis heat sinks (i.e. hydrothermal circulation; Morton and Sleep, 1985). The results of both stages are combined to yield a complete temperature distribution. Throughout, we have assumed that the zone of interest has a width of ±35 km, which is symmetric about the ridge axis.

The calculated temperature field is used to determine the depth of the brittle-plastic transition for a basaltic rock (Byerlee, 1978). Failure by normal faulting is given by

$$\sigma_1-\sigma_3=\frac{R'-1}{R'}\rho g z(1-\lambda) \tag{3}$$

where σ_1 and σ_3 are the maximum and minimum principal stresses, $R'=\sigma_1/\sigma_3$, and λ is the pore fluid factor (Sibson, 1974; Brace and Kohlstedt, 1980; Ranalli, 1995). Plastic deformation is governed by the steady state, temperature-dependent creep law

$$\dot{\varepsilon}=A(\sigma_1-\sigma_3)^n\exp\left(\frac{-Q}{RT}\right) \tag{4}$$

where $\dot{\varepsilon}$ is the uniaxial strain rate, A is a material strength constant, n is a dimensionless exponent, Q is the activation energy for creep, R is the gas constant, and T is the temperature in Kelvin (Table 1; Goetze and Evans, 1979; Kirby, 1983).

The on- and off-axis distribution of hydrothermal circulation has a significant effect on the calculated temperature field. Maximum fluid temperatures observed at seafloor vents along the Mid-Atlantic Ridge are ~325 °C, yielding a lower bound for the crustal temperature through which seawater passes (e.g. Charlou et al., 2000). The episodic nature of high-temperature circulation means that heat exchange between rising fluids and the surrounding crust is not efficient (i.e. convective cells are not stable on geologic time scales; Baker and Massoth, 1987; Baker et al., 1989). As a result, discrete heat sinks are used to represent hydrothermal circulation. At slow spreading ridges, hydrothermal fluids can penetrate deep within the crust. Calcium-in-olivine geospeedometry of gabbros drilled at the Southwest Indian Ridge suggests that there is no discernible decrease in cooling rate with depth (Coogan et al., 2007). Similar observations from the Semail ophiolite, where the spreading rate was probably faster, suggest that the whole crust is cooled by hydrothermal circulation (Van Tongeren et al., 2008). Therefore, we have allowed heat sinks to extend to the base of the crust.

Initially, the temperature field is calculated by concentrating latent heat effects at the ridge axis and by ignoring heat sinks (i.e. hydrothermal activity). Heat sinks are then added within a 1 km wide corridor, which extends down to the base of the crust. The total (i.e. vertically integrated) heat removed is distributed so that the summed magnitude of the sinks decreases exponentially away from the ridge axis (Henstock et al., 1993; Maclennan et al., 2004). This approach yields a spatial temperature distribution, which determines the strength envelope.

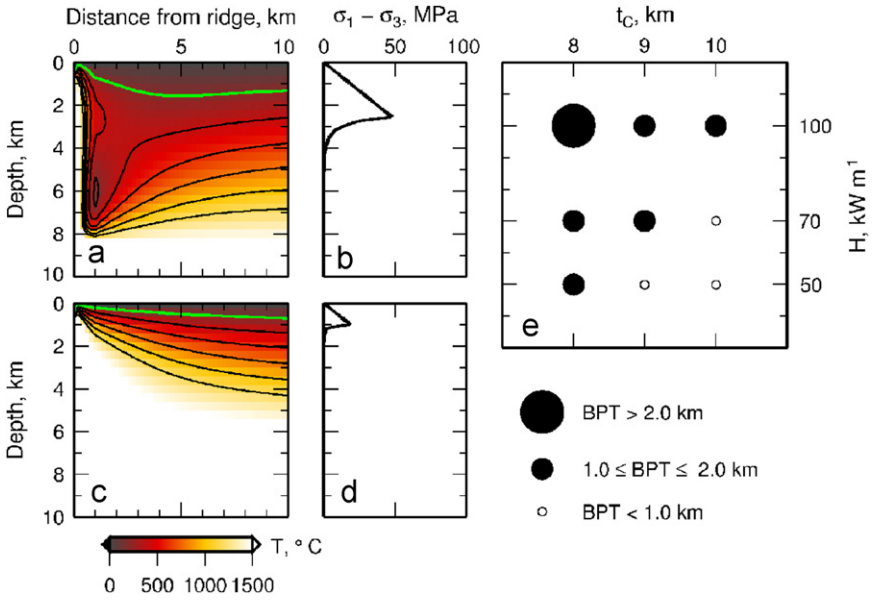

Fig. 8. Thermomechanical model of Reykjanes Ridge. (a) Calculated temperature field (crustal thickness = 8 km, asthenospheric temperature = 1330 °C, total hydrothermal cooling = 100 kW m^{-1}). Green contour = ~200 °C isotherm. (b) Stress envelope calculated from temperature field shown in (a) at a distance of 5 km from ridge. (c) Calculated temperature field (crustal thickness = 10 km, asthenospheric temperature = 1355 °C, total hydrothermal cooling = 100 kWm^{-1}). Green contour = ~200 °C isotherm. (d) Stress envelope calculated from temperature field shown in (c) at a distance 5 km from ridge crest. (e) Depth to brittle-plastic transition (BPT) for suite of nine models where crustal thickness, t_c, and total hydrothermal cooling, H, are varied. Open/closed circles scaled as shown. (For interpretation of the references to color in this figure legend, the reader is referred to the web version of this article.)

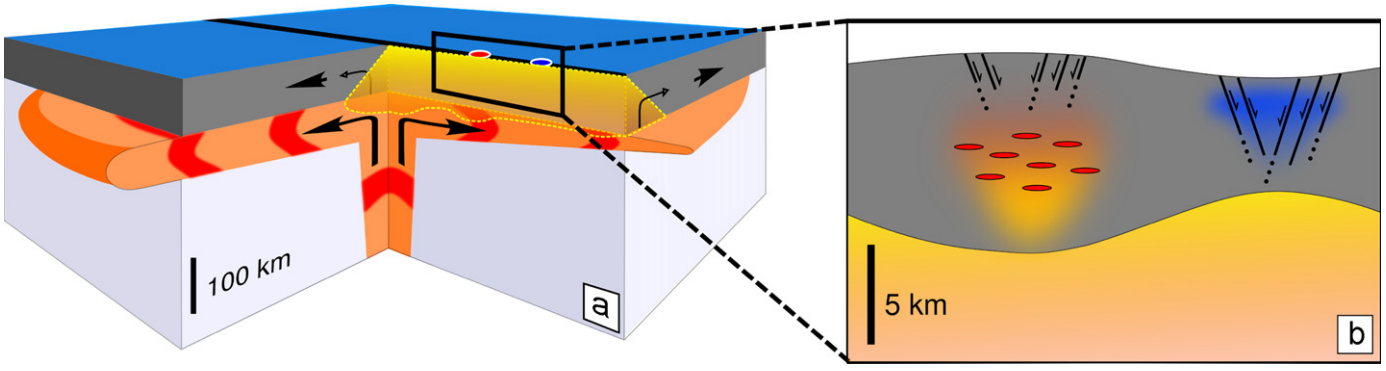

Fig. 9. (a) Cut-away cartoon showing interaction between Icelandic Plume and Reykjanes Ridge (Poore et al., 2011). Orange/red body, plume material flowing beneath lithosphere within which pulses of hotter than average material expand radially by Poiseuille flow at ~40 cm/yr (Poore et al., 2009); blue/gray block, lithosphere; black line, Reykjanes Ridge straddling plume; red/blue loci as in Fig. 7; cut-away yellow prism, melting zone under Reykjanes Ridge beneath which hot pulses travel; black arrows, plate motion, plume flow, and corner flow within melting zone. (b) Zoom showing crustal geometry above and beyond hot pulse. Gray block, oceanic crust; yellow block, high viscosity melting prism which separates crust from asthenospheric channel; black lines with arrows, idealized pattern of normal faulting; red blobs and orange shading, idealized distribution of melt within hot, thickened crust; blue shading, idealized extent of hydrothermal circulation within cold, thin crust. (For interpretation of the references to color in this figure legend, the reader is referred to the web version of this article.)

7.1. Results

To investigate the effects of along-axis changes in heat input and removal, we have calculated a suite of models for different crustal thicknesses, which reflect changes in potential temperature, and for different amounts of hydrothermal circulation. When oceanic crustal thickness increases from 8 to 10 km for a total hydrothermal cooling of 100 kW m^{-1}, there is a twofold decrease in the depth to the brittle-plastic transition (Fig. 8). This decrease occurs for several reasons. First, thicker crust is generated by a higher potential temperature and represents a larger temperature anomaly which also cools slowly since it produces more latent heat. Second, the total hydrothermal cooling is distributed over a greater depth (Fig. 9).

The rheological properties of a material are principally controlled by the homologous temperature, τ, which is the ratio of the temperature of a material to that of its melting point, both measured in Kelvin (Ashby and Verrall, 1977; Weertman, 1978). A material can only maintain stresses over geologic time if $\tau < 0.4$. For a basaltic rock, $\tau = 0.4$ corresponds to a temperature of ~200 °C (Coogan et al., 2001). This rough estimate agrees with the depth predicted by our thermomechanical model (Fig. 8).

A larger suite of thermomechanical models have been investigated, in which crustal thickness and total hydrothermal cooling are systematically varied (Fig. 8e; Supplementary Fig. 1). For a given distribution of hydrothermal cooling, the depth to the brittle-plastic transition decreases when crustal thickness increases from 8 to 10 km. Thus normal faulting plays a less important role in accommodating strain when the crust is hot and thick.

8. Discussion

The planform of the Icelandic Plume dominates the North Atlantic Ocean. It extends from Baffin Bay to Western Norway and from Spitzbergen to Newfoundland (Jones et al., 2002a). This plume is transected by a mid-oceanic ridge which acts as a linear sampler of plume activity through time (Ito, 2001; Searle et al., 1998). A history of this activity is recorded by V-shaped ridges and troughs which straddle both the Reykjanes Ridge and the Kolbeinsey Ridge. Previously, detailed analyses of these ridges and troughs suggest that they are generated by transient thermal anomalies which are generated at the base of, or within, the conduit of the plume. When they reach the base of the nascent lithosphere, it is assumed that these anomalies spread out radially within a low viscosity channel (Rudge et al., 2008).

The tip of the youngest V-shaped ridge intersects the Reykjanes Ridge $\sim$500 km southeast of Iceland where different crustal observations allow the thermal and rheological effects of a thermal anomaly beneath a mid-oceanic ridge to be investigated. Along the Reykjanes Ridge, systematic crustal changes coincide with the intersection between the youngest V-shaped ridge and the spreading axis at 60°N. The abundance of seamounts at this intersection suggests that the supply of melt to the surface is probably greater. A predominance of smooth seamounts along this part of the ridge is also striking. Hummocky seamounts with bulbous outgrowths tend to form when eruption rates are low and cooling of the surface is rapid. Smoother seamounts form when eruptions rates are higher and cooling of the surface is slower (Smith et al., 1995). Seamount morphology can also depend upon other factors but the overall morphology in a given area is primarily controlled by eruption rate (Magde and Smith, 1995; Cann and Smith, 2005). Although the seismic reflection evidence is scrappy, changes in the thickness and character of layer 2A are consistent with this inference. These morphologic observations are corroborated by crustal thickness and geochemical changes which strongly favor a greater degree of decompression melting along this segment of the Reykjanes Ridge. Further north, the abundance of seamounts decreases dramatically which suggests that this zone of increased melting is not simply a consequence of proximity to the Icelandic Plume.

Along-axis changes in magmatism are consistent with the pattern of faulting. At the tip of the youngest V-shaped ridge, there is a marked decrease in the number of mappable normal faults. This decrease coincides with a pronounced gap in earthquake activity. The estimated thickness of the brittle lid implies that faulting is largely inhibited where the V-shaped ridge is forming. Thermomechanical modeling demonstrates that a twofold decrease in the thickness of this brittle lid is achievable by generating thicker oceanic crust from decompression melting of asthenosphere, which is 25° hotter than ambient plume material. This effect is moderated by hydrothermal circulation. Since plate spreading does not change along the ridge, a greater degree of melting reduces the amount of normal faulting. If there are fewer faults, hydrothermal circulation is suppressed and the newly formed crust cools more slowly which delays thickening of the brittle lid. This positive feedback mechanism promotes the development of a tectonically quiescent segment of ridge.

Along the Kolbeinsey Ridge to the north of Iceland, a similar gap in seismicity occurs at the same radial distance from the center of the Icelandic Plume (Fig. 1a; Shorttle et al., 2010). We suggest that this gap is caused by northward flow of the same transient thermal anomaly. There are three reasons for this assertion. First, it is unlikely that the occurrence of seismic gaps at similar radial distances is a coincidence. Secondly, the gap on the Kolbeinsey Ridge occurs north of a portion of mid-oceanic ridge with a positive gravity anomaly which lacks a median valley. The crustal thickness along this ridge decreases from 12.1 ± 0.4 km to 9.5 ± 0.1 km (Hooft et al., 2006). The northern edge of the seismic gap roughly coincides with a negative gravity anomaly along the mid-oceanic ridge which is consistent with the presence of a median valley. The southern end of this median valley has a crustal thickness of 8–9 km (Kodaira et al., 1997). Finally, Jones et al. (2002b) used free-air gravity anomalies to map out V-shaped ridges and troughs which straddle the Kolbeinsey Ridge. The youngest ridge, which they labeled '1', has a similar morphology and age–distance relationship as the youngest V-shaped ridge on the opposite side of Iceland.

The evidence for radial symmetry on either side of the Icelandic Plume implies that V-shaped ridges and troughs are unlikely to be generated by channel flow beneath the mid-oceanic ridges. Instead, this symmetry suggests that transient thermal perturbations spread out radially away from the plume conduit (Shorttle et al., 2010).

9. Conclusions

We present bathymetric and seismic data, which were acquired at the Reykjanes Ridge between 60°N and 62°N, where the tip of the youngest V-shaped ridge occurs. Analysis of these data builds upon the pioneering work of Searle et al. (1998) and White et al. (1995), who suggested that a thermal anomaly lies beneath the ridge and influences a local crustal architecture. For example, between 59.5°N and 61.5°N, the density of seamounts is greater and the amount of normal faulting is diminished. This location coincides with a gap in earthquake seismicity, with a change in the geochemistry of basaltic rocks, and with a change in the crustal thickness. Thermomechanical modeling suggests that a temperature anomaly of 25 °C can account for these different observations. For example, the gap in seismicity and the regional pattern of faulting are explained by a twofold decrease in the thickness of the brittle, seismogenic layer. This decrease is consistent with estimates of rupture radii determined from a catalog of teleseismic earthquakes. Our results have important implications for crustal accretion at slow spreading mid-oceanic ridges.

A gap in seismicity occurs at a similar radial distance to the north of Iceland. The simplest explanation is that a transient thermal anomaly traveled up the plume conduit beneath Iceland and spread radially out to distances of $\sim$1000 km. Previous work has argued that the pattern of V-shaped ridges and troughs on older oceanic crust suggests that this form of transient plume activity is long lived. There is increasing evidence that this activity has had important and unexpected influences throughout the North Atlantic region. For example, ancient ephemeral landscapes emerged periodically at the fringes of the oceanic basin whose origins may be attributable to the Icelandic Plume.

Acknowledgments

R.P.T. was supported by the Girdler Fund, University of Cambridge. We thank the master, crew, technicians and scientists who contributed to the success of cruise JC50 on RRS *James Cook*. Schlumberger and Caris permitted use of their seismic and bathymetric processing software packages, respectively. Roger Searle generously provided access to multibeam bathymetric and magnetic surveys acquired on cruise CD87. We thank A. Copley, K. Czarnota, I. Frame, J. Jackson, M. Parsons, G. Roberts and J. Rudge for their help. D. Bohnenstiehl wrote a helpful review. This work was supported by Natural Environment Research Council Grant NE/G007632/1. Cambridge Earth Sciences Contribution Number esc.2639.

Appendix A. Thermal model

Asthenospheric material with a temperature of T_l upwells at the mid-oceanic ridge (Sleep, 1975; Morton and Sleep, 1985). This material follows a sub-solidus adiabatic gradient, θ, from the base of the column, z_l=100 km, to a depth of z_s=80 km where the solidus is intersected. The latent heat, L, in this region is assumed to be negligible. Between the solidus and the liquidus, the melting point gradient, β, is assumed to be constant. Between the liquidus and the surface (i.e. within oceanic crust of thickness t_c), a super-liquidus adiabatic gradient, α, is tracked. Latent heat is assumed to be released uniformly within the crust as it cools.

Following Davis and Lister (1974) and Sleep (1974), conservation of energy requires that horizontal heat flux balances excess heat generated by intrusions and so

$$-k\frac{\partial T}{\partial x}+u\rho cT=u\rho c\left(\frac{T_l z}{z_l}\right)+S(z) \tag{A.1}$$

where k is the thermal conductivity, u is the half-spreading rate, ρ is the density, c is the specific heat capacity and $S(z)$ is a function that describes heat generated by intrusions. The appropriate boundary conditions are

$$T=0,\quad z=0 \tag{A.2a}$$

$$T=T_l,\quad z=z_l \tag{A.2b}$$

$$T\to\frac{T_l z}{z_l},\quad x\to\infty \tag{A.2c}$$

Following Sleep (1975), Eq. (2) is solved by Fourier expansion which yields

$$T=\left(\frac{1}{u\rho c}\right)\sum_{m=1}^{\infty}A_m B_m\sin\left(\frac{m\pi z}{z_l}\right)\exp(a_m x)+\frac{T_l z}{z_l} \tag{A.3}$$

where A_m, B_m and a_m are given by

$$A_m\equiv 2\left(1+\sqrt{1+\frac{4\kappa^2\pi^2m^2}{u^2z_l^2}}\right)^{-1} \tag{A.4a}$$

$$\begin{aligned}B_m=\frac{2u\rho c}{m\pi}&\left\{\cos\left(\frac{m\pi z_s}{z_l}\right)\left[\left(1-\frac{z_s}{z_l}\right)T_l\gamma-T_s+T_l\left(\frac{z_s}{z_l}\right)\right]\right.\\&+\frac{\sin}{m\pi}\left(\frac{m\pi z_s}{z_l}\right)(T_l\gamma+\beta z_l-T_l)\\&+\cos\left(\frac{m\pi t_c}{z_l}\right)\left(T_s-(z_s-t_c)\beta-\frac{L}{\rho c}-t_c\right)\\&\left.+\frac{\sin}{m\pi}\left(\frac{m\pi t_c}{z_l}\right)(\alpha z_l-\beta z_l)+\frac{L}{\rho c}(T_c-\alpha t_c)\right\}\end{aligned} \tag{A.4b}$$

$$a_m=\frac{u}{2\kappa}\left(1-\sqrt{1+\frac{4\kappa^2\pi^2m^2}{u^2z_l^2}}\right). \tag{A.4c}$$

$$\gamma=1-\left(\frac{\theta z_l}{T_l}\right) \tag{A.4d}$$

where $T_s=T(z_s)$ and $T_c=T(t_c)$.

For off-axis heat sinks, the temperature field is given by

$$T=\sum_{m=1}^{\infty}A_m B_m\sin\left(\frac{m\pi z}{z_l}\right)[C_m\exp(a_m x)+D_m\exp(b_m x)] \tag{A.5}$$

where C_m, D_m and b_m are given by

$$C_m=\frac{-D_m\left(b_m-\frac{u}{\kappa}\right)}{\left(a_m-\frac{u}{\kappa}\right)} \tag{A.6a}$$

$$D_m=\frac{Q_{ij}\exp(-b_m x_j)}{(b_m-a_m)\kappa} \tag{A.6b}$$

$$b_m=\frac{u}{2\kappa}\left(1+\sqrt{1+\frac{4\kappa^2\pi^2m^2}{u^2z_l^2}}\right) \tag{A.6c}$$

The continuous heat source term, $Q(x,z)$, in Eq. (2) is represented as a discrete sum of point sources located at a position, (x_i,z_j), from the axis

$$Q(x,z)=\sum_{i,j}Q_{ij}\delta(x-x_i)\delta(z-z_j) \tag{A.7}$$

where δ is the delta function.

Appendix B. Supplementary data

Supplementary data associated with this article can be found in the online version at http://dx.doi.org.10.1016/j.epsl.2012.12.030.

References

Appelgate, B., Shor, A.N., 1994. The northern Mid-Atlantic and Reykjanes Ridges: Spreading center morphology between 55°50′N and 63°00′N. J. Geophys. Res. 99, 17935–17956.

Ashby, M.F., Verrall, R.A., 1977. Micromechanisms of flow and fracture, and their relevance to the rheology of the upper mantle. Philos. Trans. R. Soc. Lond. A 288, 59–95.

Baker, E.T., Lavelle, J.W., Feely, R.A., Massoth, G.J., Walker, S., 1989. Episodic venting of hydrothermal fluids from the Juan de Fuca Ridge. J. Geophys. Res. 94, 9237–9250.

Baker, E.T., Massoth, G.J., 1987. Characteristics of hydrothermal plumes from two vent fields on the Juan de Fuca Ridge, northeast Pacific Ocean. Earth Planet. Sci. Lett. 85, 59–73.

Behn, M.D., Ito, G., 2008. Magmatic and tectonic extension at mid-ocean ridges: 1. Controls on fault characteristics. Geochem. Geophys. Geosyst. 9, http://dx.doi.org/10.1029/2008GC001965.

Benediktsdóttir, A., Hey, R., Martinez, F., Hoskuldsson, A., 2012. Detailed tectonic evolution of the Reykjanes Ridge during the past 15 Ma. Geochem. Geophys. Geosyst. 13, http://dx.doi.org/10.1029/2011GC003948.

Brace, W.F., Kohlstedt, D.L., 1980. Limits on lithospheric stress imposed by laboratory experiments. J. Geophys. Res. 85, 6248–6252.

Buck, W.R., Lavier, L.L., Poliakov, A.N.B., 2005. Modes of faulting at mid-ocean ridges. Nature 434, 719–723.

Byerlee, J., 1978. Friction of rocks. Pure Appl. Geophys. 116, 615–626.

Calvert, A.J., 1997. Backscattered coherent noise and seismic reflection imaging of the oceanic crust: an example from the rift valley of the Mid-Atlantic Ridge at 23°N. J. Geophys. Res. 102, 5119–5133.

Canales, J.P., Detrick, R.S., Carbotte, S.M., Kent, G.M., Diebold, J.B., Harding, A., Babcock, J., Nedimovic, M.R., 2005. Upper crustal structure and axial topography at intermediate spreading ridges: seismic constraints from the southern Juan de Fuca Ridge. J. Geophys. Res. 110, http://dx.doi.org/10.1029/2005JB003630.

Cann, J., Smith, D.K., 2005. Evolution of volcanism and faulting in a segment of the Mid-Atlantic Ridge at 25°N. Geochem. Geophys. Geosyst. 6, http://dx.doi.org/10.1029/2005GC000954.

Cazenave, A., Souriau, A., Dominh, K., 1989. Global coupling of Earth surface topography with hotspots, geoid and mantle heterogeneities. Nature 340, 54–58.

Charlou, J.L., Donval, J.P., Douville, E., Jean-Baptiste, P., Radford-Knoery, J., Fouquet, Y., Dapoigny, A., Stievenard, M., 2000. Compared geochemical signatures and the evolution of Menez Gwen (37°50′N) and Lucky Strike (37°17′N) hydrothermal fluids, south of the Azores Triple Junction on the Mid-Atlantic Ridge. Chem. Geol. 171, 49–75.

Chen, Y.J., 2003. Influence of the Iceland mantle plume on crustal accretion at the inflated Reykjanes Ridge: magma lens and low hydrothermal activity? J. Geophys. Res. 108, http://dx.doi.org/10.1029/2001JB000816.

Christeson, G.L., McIntosh, K.D., Karson, J.A., 2007. Inconsistent correlation of seismic layer 2a and lava layer thickness in oceanic crust. Nature 445, 418–421.

Coogan, L., Wilson, R.N., Gillis, K.M., MacLeod, C.J., 2001. Near-solidus evolution of oceanic gabbros: insights from amphibole geochemistry. Geochim. Cosmochim. Acta 65, 4339–4357.

Coogan, L.A., Jenkin, G.R.T., Wilson, R.N., 2007. Contrasting cooling rates in the lower oceanic crust at fast- and slow-spreading ridges revealed by geospeedometry. J. Petrol. 48, 2211–2231.

Crane, K., Johnson, L., Appelgate, B., Nishimura, C., Böning, C., Jones, C., Vogt, P.R., Yan, R.K.O.S., 1997. Volcanic and seismic swarm events on the Reykjanes Ridge and their similarities to events on Iceland: results of a rapid response mission. Mar. Geophys. Res. 19, 319–338.

Davis, E.E., Lister, C.R.B., 1974. Fundamentals of ridge crest topography. Earth Planet. Sci. Lett. 21, 405–413.

Delorey, A., Dunn, R.A., Gaherty, J.B., 2007. Surface wave tomography of the upper mantle beneath the Reykjanes Ridge with implications for ridge hot spot interaction. J. Geophys. Res. 112, http://dx.doi.org/10.1029/2006JB004785.

Einarsson, P.A., 1979. Seismicity and earthquake focal mechanisms along the mid-Atlantic plate boundary between Iceland and the Azores. Tectonophysics 55, 127–153.
Einarsson, P.A., 1991. Earthquakes and present-day tectonism in Iceland. Tectonophysics 189, 261–279.
Engdahl, E., van der Hilst, R., Buland, R., 1998. Global teleseismic earthquake relocation with improved travel times and procedures for depth determination. Bull. Seismol. Soc. Am. 88, 722–743.
Eshelby, J.D., 1957. The determination of the elastic field of an ellipsoidal inclusion, and related problems. Proc. R. Soc. Lond. A 241, 376–396.
Francis, T.J.G., 1973. The seismicity of the Reykjanes Ridge. Earth Planet. Sci. Lett. 18, 119–123.
Gee, J.S., Cande, S.C., Hildebrand, J.A., Donnelly, K., Parker, R.L., 2000. Geomagnetic intensity variations over the past 780 kyr obtained from near-seafloor magnetic anomalies. Nature 408, 827–832.
Goetze, C., Evans, B., 1979. Stress and temperature in the bending lithosphere as constrained by experimental rock mechanics. Geophys. J. Int. 59, 463–478.
Hager, B.H., Clayton, R.W., Richards, M.A., Comer, R.P., Dziewonski, A.M., 1985. Lower mantle heterogeneity, dynamic topography and the geoid. Nature 313, 541–545.
Hager, B.H., Richards, M.A., 1989. Long-wavelength variations in Earth's geoid: physical models and dynamical implications. Philos. Trans. R. Soc. Lond. A 328, 309–327.
Hanks, T., 1977. Earthquake stress drops, ambient tectonic stresses and stresses that drive plate motions. Pure Appl. Geophys. 115, 441–458.
Hanks, T., Boore, D., 1984. Moment-magnitude relations in theory and practice. J. Geophys. Res. 89, 6229–6235.
Hanks, T., Kanamori, H., 1979. A moment magnitude scale. J. Geophys. Res. 84, 2348–2350.
Harding, A.J., Kent, G.M., Orcutt, J., 1993. A multichannel seismic investigation of upper crustal structure at 9°N on the East Pacific Rise: implications for crustal accretion. J. Geophys. Res. 98, 13,925–13,944.
Hartley, R.A., Roberts, G.G., White, N.J., Richardson, C., 2011. Transient convective uplift of an ancient buried landscape. Nat. Geosci. 4, 562–565.
Henstock, T., Woods, A., White, R.S., 1993. The accretion of oceanic crust by episodic sill intrusion. J. Geophys. Res. 98, 4143–4161.
Hey, R., Martinez, F., Höskuldsson, A., Benediktsdóttir, A., 2010. Propagating rift model for the V-shaped ridges south of Iceland. Geochem. Geophys. Geosyst. 11, http://dx.doi.org/10.1029/2009GC002865.
Hooft, E.E.E., Brandsdóttir, B., Mjelde, R., Shimamura, H., Murai, Y., 2006. Asymmetric plume–ridge interaction around Iceland: the Kolbeinsey Ridge Iceland seismic experiment. Geochem. Geophys. Geosyst. 7, http://dx.doi.org/10.1029/2005GC001123.
Huang, P., Solomon, S., 1988. Centroid depths of Mid-Ocean Ridge earthquakes: dependence on spreading rate. J. Geophys. Res. 93, 13445–13477.
Ito, G., 2001. Reykjanes 'V'-shaped ridges originating from a pulsing and dehydrating mantle plume. Nature 411, 681–684.
Ito, G., Behn, M.D., 2008. Magmatic and tectonic extension at mid-ocean ridges: 2. Origin of axial morphology. Geochem. Geophys. Geosyst. 9, http://dx.doi.org/10.1029/2008GC001970.
Jones, S.M., Maclennan, J., Murton, B.J., Godfrey Fitton, J., White, N.J., 2010. New joint geochemical–geophysical record of time-dependent mantle convection south of Iceland. Abstract U44A-07 Presented at 2010 Fall Meeting, AGU, San Francisco, CA, 13–17 December.
Jones, S.M., White, N.J., Clarke, B.J., Rowley, E., Gallagher, K., 2002a. Present and past influence of the Iceland plume on sedimentation. Geol. Soc. Spec. Pub. 196, 13–25.
Jones, S.M., White, N.J., Lovell, B., 2001. Cenozoic and Cretaceous transient uplift in the Porcupine Basin and its relationship to a mantle plume. Geol. Soc. Spec. Pub. 188, 345–360.
Jones, S.M., White, N.J., Maclennan, J., 2002b. V-shaped ridges around Iceland: implications for spatial and temporal patterns of mantle convection. Geochem. Geophys. Geosyst. 3, http://dx.doi.org/10.1029/2002GC000361.
Kanamori, H., 1983. Magnitude scale and quantification of earthquakes. Tectonophysics 93, 185–199.
Keeton, J., Searle, R.C., Peirce, C., Parsons, B., 1997. Bathymetry of the Reykjanes Ridge. Mar. Geophys. Res. 19, 55–64.
Kent, D.V., Gee, J., 1996. Magnetic alteration of zero-age oceanic basalt. Geology 24, 703–706.
Kirby, S., 1983. Rheology of the lithosphere. Rev. Geophys. 21, 1458–1487.
Klitgord, K., 1976. Sea-floor spreading: the central anomaly magnetization high. Earth Planet. Sci. Lett. 29, 201–209.
Kodaira, S., Mjelde, R., Gunnarsson, K., Shiobara, H., Shimamura, H., 1997. Crustal structure of the Kolbeinsey ridge, North Atlantic, obtained by use of ocean bottom seismographs. J. Geophys. Res. 102, 3131–3151.
Lee, S.M., Searle, R.C., 2000. Crustal magnetization of the Reykjanes Ridge and implications for its along-axis variability and the formation of axial volcanic ridges. J. Geophys. Res. 105, 5907–5930.
Levi, S., Audunsson, H., Duncan, R.A., Kristjansson, L., Gillot, P.Y., Jakobsson, S.P., 1990. Late Pleistocene geomagnetic excursion in Icelandic lavas: confirmation of the Laschamp excursion. Earth Planet. Sci. Lett. 96, 443–457.
Maclennan, J., Hulme, T., Singh, S., 2004. Thermal models of oceanic crustal accretion: linking geophysical, geological and petrological observations Geochem. Geophys. Geosyst. 5, http://dx.doi.org/10.1029/2003GC000605.
Magde, L.S., Smith, D.K., 1995. Seamount volcanism at the Reykjanes Ridge: relationship to the Iceland hot spot. J. Geophys. Res. 100, 8449–8468.
Marshall, M., Cox, A., 1972. Magnetic changes in pillow basalt due to sea floor weathering. J. Geophys. Res. 77, 6459–6469.
Morton, J.L., Sleep, N.H., 1985. A Mid-Ocean Ridge thermal model: constraints on the volume of axial hydrothermal heat flux. J. Geophys. Res. 90, 11345–11353.
Murton, B.J., Taylor, R.N., Thirwall, M.F., 2002. Plume–ridge interaction: a geochemical perspective from the Reykjanes Ridge. J. Petrol. 43, 1987–2012.
Parnell-Turner, R.E., White, N.J., Henstock, T., Maclennan, J., Murton, B.J., Jones, S.M., 2011. 40 million years of the Iceland plume. Abstract T11D-02 presented at 2011 Fall Meeting, AGU, San Francisco, CA, 5–9 December.
Peirce, C., Sinha, M.C., Topping, S., Gill, C., 2007. Morphology and genesis of slow-spreading ridges-seabed scattering and seismic imaging within the oceanic crust. Geophys. J. Int. 168, 59–89.
Poore, H.R., Samworth, R., White, N.J., Jones, S.M., McCave, I.N., 2006. Neogene overflow of northern component water at the Greenland–Scotland Ridge. Geochem. Geophys. Geosyst. 7, http://dx.doi.org/10.1029/2005GC001085.
Poore, H.R., White, N.J., Jones, S.M., 2009. A Neogene chronology of Iceland plume activity from V-shaped ridges. Earth Planet. Sci. Lett. 283, 1–13.
Poore, H.R., White, N.J., Maclennan, J., 2011. Ocean circulation and mantle melting controlled by radial flow of hot pulses in the Iceland plume. Nat. Geosci. 4, 558–561.
Ranalli, G., 1995. Rheology of the Earth. Chapman & Hall.
Rudge, J.F., Shaw Champion, M.E., White, N.J., McKenzie, D.P., Lovell, B., 2008. A plume model of transient diachronous uplift at the Earth's surface. Earth Planet. Sci. Lett. 267, 146–160.
Sandwell, D.T., Smith, W.H.F., 2009. Global marine gravity from retracked Geosat and ERS-1 altimetry: ridge segmentation versus spreading rate. J. Geophys. Res. 114, http://dx.doi.org/10.1029/2008JB006008.
Schubert, G., Olson, P., 1989. Solitary waves in mantle plumes. J. Geophys. Res. 94, 9523–9532.
Schubert, G., Turcotte, D.L., Olson, P., 2001. Mantle Convection in the Earth and Planets. Cambridge University Press.
Searle, R.C., Field, P., Owens, R., 1994. Segmentation and a nontransform ridge offset on the Reykjanes Ridge near 58°N. J. Geophys. Res. 99, 24159–24172.
Searle, R.C., Keeton, J., Owens, R., White, R.S., Mecklenburgh, R., Parsons, B., Lee, S.M., 1998. The Reykjanes Ridge: structure and tectonics of a hot-spot-influenced, slow-spreading ridge, from multibeam bathymetry, gravity and magnetic investigations. Earth Planet. Sci. Lett. 160, 463–478.
Shorttle, O., Maclennan, J., 2011. Compositional trends of Icelandic basalts: implications for short length scale lithological heterogeneity in mantle plumes. Geochem. Geophys. Geosyst. 12, http://dx.doi.org/10.1029/2011GC003748.
Shorttle, O., Maclennan, J., Jones, S.M., 2010. Control of the symmetry of plume–ridge interaction by spreading ridge geometry. Geochem. Geophys. Geosyst. 11, http://dx.doi.org/10.1029/2009GC002986.
Sibson, R.H., 1974. Frictional constraints on thrust, wrench and normal faults. Nature 249, 542–544.
Sleep, N.H., 1974. Segregation of magma from a mostly crystalline mush. Geol. Soc. Am. Bull. 85, 1225–1232.
Sleep, N.H., 1975. Formation of oceanic crust: some thermal constraints. J. Geophys. Res. 80, 4037–4042.
Smallwood, J.R., White, R.S., 1998. Crustal accretion at the Reykjanes Ridge. J. Geophys. Res. 103, 5185–5201.
Smith, D.K., Cann, J., 1992. The role of seamount volcanism in crustal construction at the Mid-Atlantic Ridge (24–30°N). J. Geophys. Res. 97, 1645–1658.
Smith, D.K., Cann, J., Dougherty, M., Lin, J., Spencer, S., Macleod, C.J., Keeton, J., McAllister, E., Brooks, B., Pascoe, R., 1995. Mid-Atlantic Ridge volcanism from deep-towed side-scan sonar images, 25–29°N. J. Volcanol. Geoth. Res. 67, 233–262.
Toomey, D., Solomon, S., Purdy, G., Murray, M., 1985. Microearthquakes beneath the median valley of the Mid-Atlantic Ridge near 23°N: hypocenters and focal mechanisms. J. Geophys. Res. 90, 5443–5458.
Van Tongeren, J.A., Kelemen, P.B., Hanghøj, K., 2008. Cooling rates in the lower crust of the Oman ophiolite: Ca in olivine, revisited. Earth Planet. Sci. Lett. 267, 69–82.
Vera, E.E., Mutter, J.C., Buhl, P., Orcutt, J.A., Harding, A.J., Kappus, M.E., Detrick, R.S., Brocher, T.M., 1990. The structure of 0- to 0.2-m.y.-old oceanic crust at 9°N on the East Pacific Rise from expanded spread profiles. J. Geophys. Res. 95, 15,529–15,556.
Vogt, P.R., 1971. Asthenospehere motion recorded by the ocean floor south of Iceland. Earth Planet. Sci. Lett. 13, 153–160.
Weertman, J., 1978. Creep laws for the mantle of the Earth. Phil. Trans. R. Soc. Lond. A. 288, 9–26.
White, R.S., 1997. Rift–plume interaction in the North Atlantic. Philos. Trans. R. Soc. Lond. A 355, 319–339.
White, R.S., Bown, J., Smallwood, J.R., 1995. The temperature of the Iceland plume and origin of outward-propagating V-shaped ridges. J. Geol. Soc. 152, 1039–1045.
Wiens, D.A., Stein, S., 1983. Age dependence of oceanic intraplate seismicity and implications for lithospheric evolution. J. Geophys. Res. 88, 6455–6468.
Wright, J.D., Miller, K.G., 1996. Greenland–Scotland Ridge control of North Atlantic Deep Water. Paleoceanography 11, 157–170.
Zhou, W., Voo, R.V.D., Peacor, D.R., Zhang, Y., 2000. Variable Ti-content and grain size of titanomagnetite as a function of cooling rate in very young MORB. Earth Planet. Sci. Lett. 179, 9–20.